Wolf-Rayet Stars
W.-R. Hamann, A. Sander, H. Todt, eds.
Potsdam: Univ.-Verlag, 2015
URL: http://nbn-resolving.de/urn:nbn:de:kobv:517-opus4-84268

Wind models and spectral analyses

W.-R. Hamann[1] and the Potsdam group
[1] *Universität Potsdam, Germany*

The emission-line dominated spectra of Wolf-Rayet stars are formed in expanding layers of their atmosphere, i.e. in their strong stellar wind. Adequate modeling of such spectra has to face a couple of difficulties. Because of the supersonic motion, the radiative transfer is preferably formulated in the co-moving frame. The strong deviations from local thermodynamical equilibrium (LTE) require to solve the equations of statistical equilibrium for the population numbers, accounting for many hundred atomic energy levels and thousands of line transitions. Moreover, millions of lines from iron-group elements must be taken into account for their blanketing effect. Model atmospheres of the described kind can reproduce the observed WR spectra satisfyingly, and have been widely applied for corresponding spectral analyses.

1 Expanding atmospheres

The spectra of Wolf-Rayet stars are characterized by bright and broad emission lines, which are formed in their rapidly expanding atmosphere (Beals 1929). These emission lines are mainly powered by recombination cascades. The line width reflects the range of Doppler shifts which the lines-of-sight can encounter (Fig. 1).

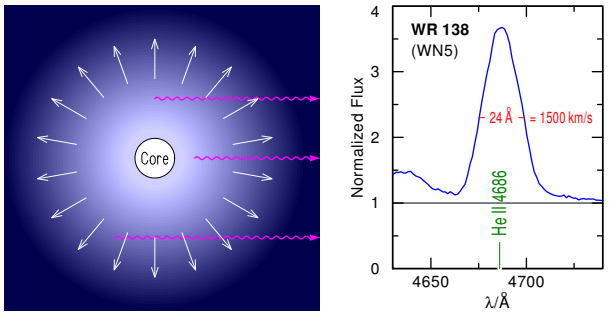

Fig. 1: Sketch of a spherical stellar wind *(left)*, which leads to the formation of broad emission lines *(right)*.

In order to analyze such spectra quantitatively, adequate models are prerequisite. Two major complications make this a non-trivial task: the strong deviations from local thermodynamical equilibrium (non-LTE), and the supersonic expansion.

In non-LTE, the population numbers of the various atomic energy levels must be calculated from the *rate equations*, i.e. from balancing all collisional and radiative transitions that are relevant. Each radiative rate has to be calculated from the local radiation field at the frequencies of the corresponding transition, as seen in the co-moving frame of reference (CMF) of the considered volume element.

Thus, the other part of the task is to calculate the radiation field. In the CMF, a propagating ray of light is continuously changing its CMF frequency due to the differential motion of the medium (cf. Fig. 2). Therefore the radiative transfer in the CMF is described by a set of *partial* differential equations which contain also frequency derivatives,

$$\frac{\partial I_\nu}{\partial z} - \frac{\nu}{c}\frac{\mathrm{d}(\vec{v}\cdot\vec{n})}{\mathrm{d}z}\,\frac{\partial I_\nu}{\partial \nu} = \varkappa\,(I_\nu - S_\nu) \quad . \qquad (1)$$

Here, I_ν denotes the specific intensity, z the spatial coordinate along the ray, and $\vec{v}\cdot\vec{n}$ the velocity projected on the ray's direction $\vec{n}$. The opacity $\varkappa$ and the source function S_ν have to be calculated at each point along the ray from the local non-LTE population numbers.

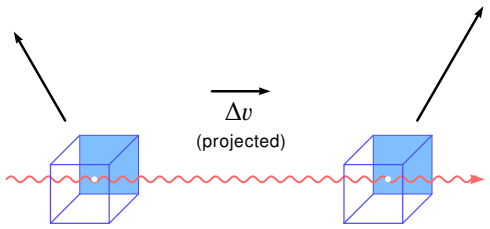

Fig. 2: Radiation transfer in the co-moving frame (CMF) for a differentially expanding atmosphere

The radiative transport couples in space, and the rate equations in frequency. For spherical symmetry, the discretization of these equations was developed in a series of papers more than 40 years ago (e.g. Mihalas et al. 1976). With the need to account for $\sim 10^3$ levels, $\sim 10^5$ frequencies, $\sim 10^2$ radial grid points and the same number of ray directions, the total problem is of high dimension. The numerical solution became only possible when the method of *approximate lambda operators* was developed (Hamann 1986).

Even with sophisticated algorithms, the number of non-LTE levels that can be treated explicitely is limited to $\sim 10^3$, mainly for reasons of numerical stability. On the other hand, iron with its many electrons provides millions of spectral lines which have a significant influence on the temperature and ionization stratification of hot-star atmospheres (so-called *iron line blanketing*). In order to take this into account, the concept of *superlevels* can be adapted (Gräfener et al. 2002), which was proposed originally by Anderson (1989).

In this approximation, the large number of atomic energy levels (termed "sublevels" in the following) is represented by a small number of "superlevels" (cf. Fig. 3). Relative populations within a superlevel are assumed to be in LTE. Each transition between two superlevels comprises a large number of atomic line transitions ("sublines"). In the radiation transport, all sublines must be treated at their proper frequency because of the frequency coupling in expanding atmospheres. Hence, in contrast to static atmospheres, no sampling or re-ordering techniques can be applied. Instead, each superline has a complicated opacity profile function which is a superposition of all sublines involved (Fig. 4).

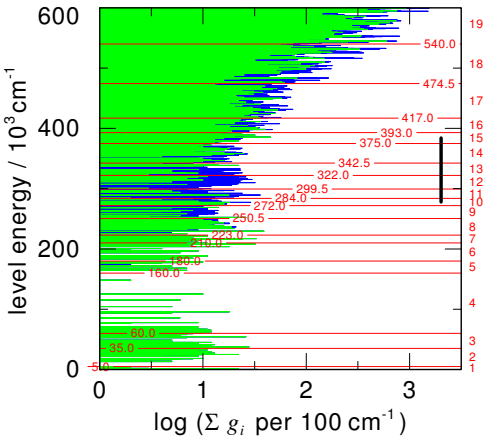

Fig. 3: Superlevel definition for Fe V (plus further iron-group elements). The horizontal stripes indicate the total statistical weight of all lines within energy bins of 100 cm^{-1} (parity coded by green and blue color, respectively). The red lines show a possible division into 19 energy bands.

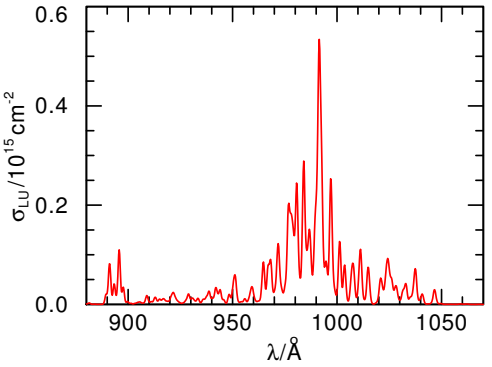

Fig. 4: Superline photo cross section for the transition between superlevels 10 and 15 in Fe V shown in Fig. 3

There is plenty of evidence that stellar winds are not homogeneous. Especially in WR spectra, such evidence is found from the electron-scattering (e.s.) wings of strong emission lines. Due to their low mass, electrons have a high thermal velocity. Radiation transfer theory therefore predicts that electron scattering causes a broad frequency redistribution of line photons (Hummer 1962; Hillier 1984). Assuming a smooth wind, however, models predict much stronger e.s. wings than observed (cf. Fig. 5).

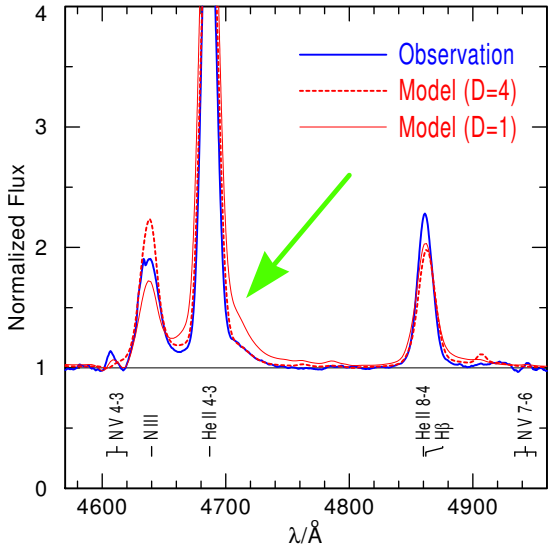

Fig. 5: Effect of electron scattering on the red wing of the strong emission line He II 4686 for the WN7 star Brey 24 in the LMC. The smooth wind model (thin red line) predicts a much stronger e.s. red wing (green arrow) than observed (blue line). With a clumping factor of D=4 and the mass-loss rate reduced by the factor $\sqrt{D}$, this wing fits the observation, while the strength of the emission lines generally remains unchanged (thick dashed red curve).

The effect of wind inhomogeneities can be taken into account in the *microclumping* approximation under the simplifying assumption that the clumps have a small size, compared to the mean free path of the photons at any frequency. In this limit, the radiation field stays smooth and can be calculated with the averaged opacities and emissivities. The rate equations, however, have to be solved for the local density. In the simplest form, we assume that wind consists of clumps with a density that is enhanced by a factor of D compared to the smooth model with same mass-loss rate, while the interclump space is void (e.g. Hamann & Koesterke 1998). Since the emission lines are powered by the recombination cascades and the recombination rate scales with the square of the density, the mass-loss rate has to be reduced by the factor $\sqrt{D}$ compared to the smooth model in order to keep the total line emission unchanged. The electron scattering, however, scales only linear with density and the corresponding line wings are therefore reduced in the clumped

model. Agreement with observations is achieved with clumping factors between 4 and 10 for typical WR stars (cf. Fig. 5). In the next step of approximation, one can account additionally for a non-void interclump medium (Zsargó et al. 2008).

Oskinova et al. (2007) pointed out that the basic assumption for the microclumping approximation is not fulfilled for strong stellar winds: clumps of plausible size are not always optically thin, neither in strong lines, nor at the strong K-shell edges in the X-ray regime. In a statistical approach, they developed a generalized formalism for such *macroclumping*. Opacities are effectively reduced by the porosity. Line transfer is especially affected, since the interaction of a photon with a line transition is anyhow restricted to those small parts of the differentially moving medium where the Doppler shift is suitable. Macroclumping can also induce inhomogeneities in the source function and temperature structure, which had to be neglected in the approximation by Oskinova et al. (2007). Nevertheless, this approach can reconcile the discrepancies between different mass-loss diagnostics (UV resonance lines versus Hα emission) found for O stars: for a given $\dot{M}$ the unsaturated P Cygni profiles become weaker.

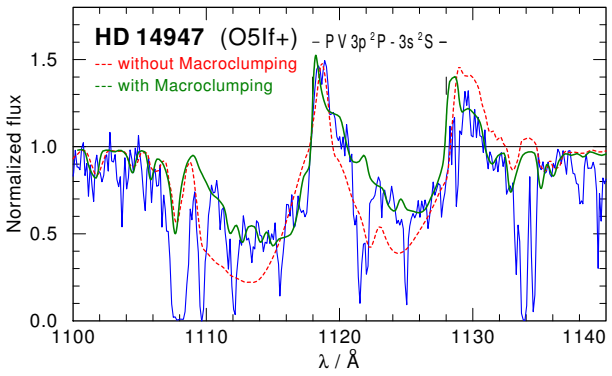

Fig. 6: The effect of macroclumping on the unsaturated P V resonance doublet in HD 14947. The FUSE observation (blue ragged line) is compared to the prediction of the standard PoWR model without macroclumping (red dashed line), and to the result from a Monte-Carlo simulation for macroclumping (green line). The mass loss rate is chosen such that Hα is fitted simultaneously with a clumping factor of D=10. Adapted from Šurlan et al. (2013)

Especially for the scattering in resonance doublets, the radiative transfer in a 3-dimensional clumped wind has been simulated with Monte-Carlo techniques (Šurlan et al. 2012, 2013) for a couple of O stars. As predicted from the statistical approach by Oskinova et al. (2007), the unsaturated P Cygni profiles become weaker by macroclumping (see Fig. 6). A similar result has now been obtained also for WR stars (Kubátova et al., these proc.).

2 Models

A "standard" WR atmosphere is assumed to be expanding in a spherically-symmetric, homogeneous and stationary flow. With a given mass-loss rate $\dot{M}$, the density stratification and the velocity field $v(r)$ are related via the equation of continuity. The velocity field in the supersonic wind is pre-specified in form of the so-called *beta law*,

$$v(r) = v_\infty \left(1 - \frac{r_0}{r}\right)^\beta \qquad (2)$$

where β is usually set to unity for WR winds. r_0 is close to the stellar radius, but its precise value must guarantee a suitable transition to the subsonic part of the atmosphere. The terminal wind velocity v_∞ is a free parameter of these models.

The "stellar radius" R_* refers by definition to the inner boundary of the model atmosphere. It became usual to locate this boundary at the Rosseland optical depth of 20. For most of the WR stars, the expansion velocity at R_* is still subsonic. Nevertheless, R_* might not be identical to the hydrostatic core radius from stellar evolution models because of the recently discovered effect of *envelope inflation* (Gräfener et al. 2012). Moreover, there is a parameter range of very thick winds where the low-velocity parts of the wind are totally hidden beyond large optical depths (see below).

The "stellar temperature" T_* is defined by the luminosity L and the stellar radius R_* via the Stefan-Boltzmann law, i.e. T_* denotes the effective temperature referring to the radius R_*. Only Doppler line broadening must be taken into account in stellar winds. The broadening velocity v_D includes the microturbulence, which turns out to be of the order of 100 km/s in WR winds.

Adopting the described "standard model" assumptions, any particular WR atmosphere is specified by its chemical composition and the basic parameters L, T_*, $\dot{M}$, v_∞. Note that such semi-empirical models are not hydrodynamically consistent. HD models for WR stars which predict $\dot{M}$ and v_∞ consistently are still in their infancy (e.g. Gräfener & Hamann 2008, Sander et al., these proceedings).

Major codes for calculating the described kind of models are CMFGEN (Hillier 2012), which is publicly available[1], and the Potsdam Wolf-Rayet (PoWR) code, from which many models are available via a web interface[2]. The more approximate code FASTWIND (e.g. Puls et al. 2005) has been applied mainly to O stars yet.

[1] kookaburra.phyast.pitt.edu/hillier
[2] www.astro.physik.uni-potsdam.de/PoWR

3 Spectral analyses

With models as described in the previous section, one can usually achieve a satisfactory fit to the observations, regarding the spectral energy distribution as well as the line spectrum. An example is shown in Figs. 7+8 for the Galactic WR star WR 24 (WN6ha) (adapted from Hamann et al. 2006). As result of such an iterative fit procedure, the stellar and wind parameters are empirically determined.

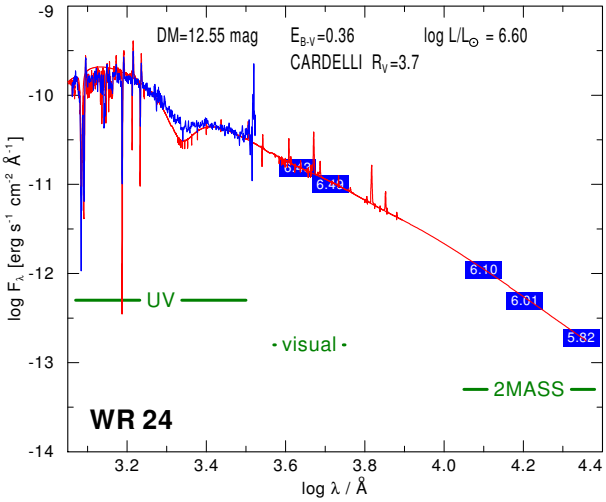

Fig. 7: Fit of a PoWR model to the spectral energy distribution (SED) of the WN6 star WR24. The luminosity and the reddening parameter are adjusted such that the observation (blue) is matched.

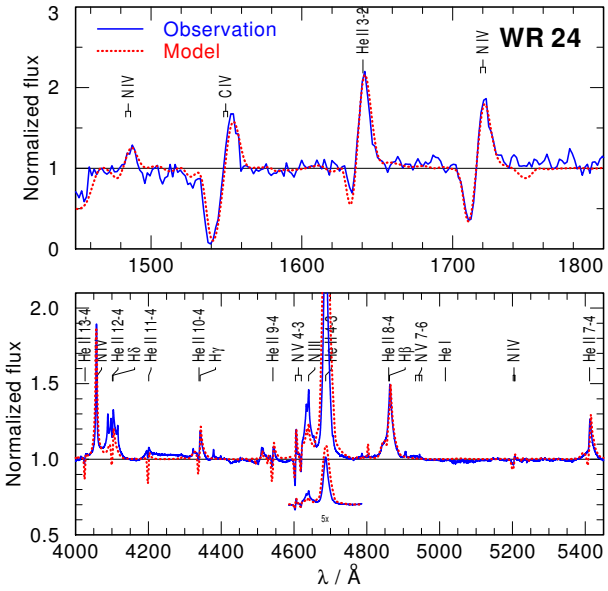

Fig. 8: Fit to the observed line spectrum of WR 24 in the UV and optical

Such analyses are facilitated by the fact that the emission line spectra of WR stars depend mainly on two parameters only, the stellar temperature T_* and a combination of radius, mass-loss rate, and wind velocity. For the latter combination, Schmutz et al. (1989) defined

$$R_t = R_* \left[\frac{v_\infty}{2500\,\mathrm{km\,s^{-1}}} \Big/ \frac{\dot{M}\sqrt{D}}{10^{-4}\,M_\odot\,\mathrm{yr}^{-1}} \right]^{2/3} \qquad (3)$$

and termed this quantity (misleadingly) the "transformed radius". Only later it was realized that R_t is related to the emission measure, normalized to the area of the stellar surface. Anyhow, models with the same R_t show approximately the same normalized line spectrum, while the absolute model flux just scales with the luminosity. Therefore, analyses of WR spectra can be based on a model grid in the $T_* - R_t$ plane which is calculated for only one typical luminosity and v_∞. As an example, Fig. 9 shows the contours of constant equivalent width for a grid of WC models in this parameter plane.

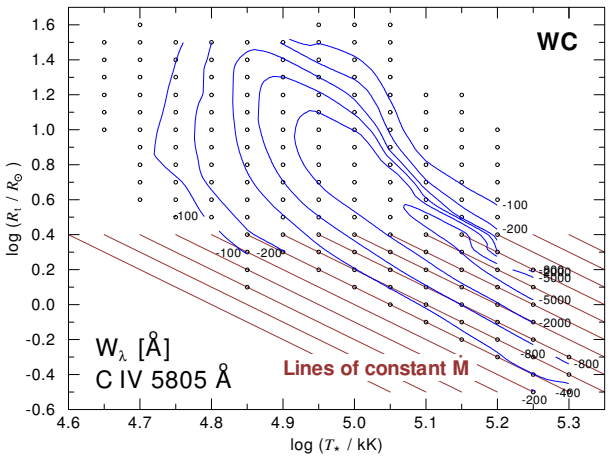

Fig. 9: Contours of constant equivalent width of the C IV line at 5805 Å, labeled with W_λ in Å for the PoWR grid of Galactic WC star models

Fig. 9 illustrates a further parameter degeneracy, which is encountered for the densest WR winds ($\log(R_t/R_\odot) \lesssim 0.4$). In this part of the $\log T_* - \log R_t$ plane, all contour lines become approximately parallel to lines of constant mass-loss rate (brown parallel lines). The spectra then depend only on the ratio $L/\dot{M}^{3/4}$, while neither T_* nor R_* play any role. One can easily understand this when imagining a wind that is so dense that all visible layers expand already with the terminal velocity. Such model is completely determined by this velocity, the luminosity, and the mass-loss rate. The $R_t - T_*$ diagram for the Galactic WN stars (Fig. 10) shows that a couple of stars with earliest subtypes and strong lines (mainly WN4-6s) fall into the domain of this degeneracy where only lower limits for T_* can be derived spectroscopically.

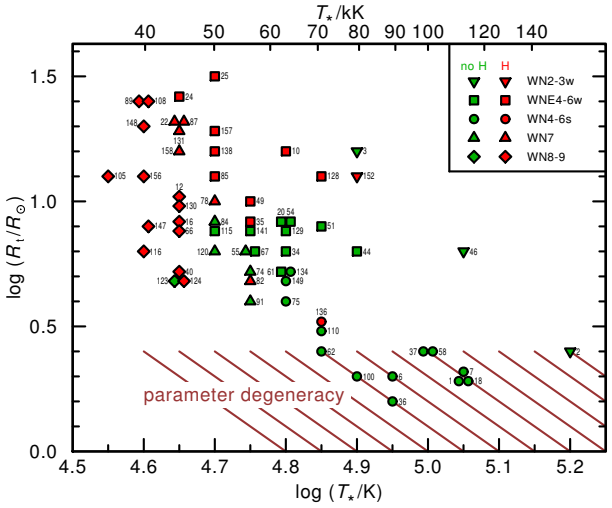

Fig. 10: Location of the Galactic WN stars in the $R_t - T_*$ plane. Red and green symbols indicate whether hydrogen is detectable or absent in their atmosphere, respectively. The shape of the symbol codes the spectral subtype (see inlet). Adapted from Hamann et al. (2006)

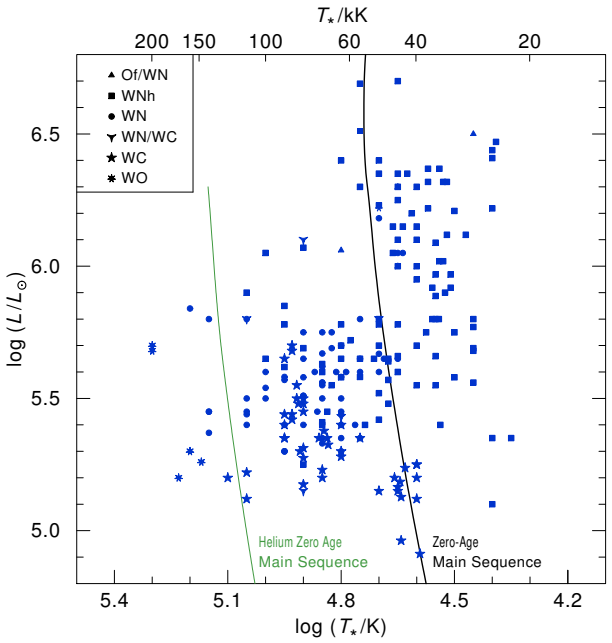

Fig. 11: HRD with the locations of WR stars as obtained from spectral analyses with atmosphere models, compiled from various sources (Crowther et al. 2002; Hamann et al. 2006; Barniske et al. 2008; Martins et al. 2008; Liermann et al. 2010; Sander et al. 2012, 2014; Hainich et al. 2014, 2015; Tramper et al. 2013, 2015)

Up to now, more than 250 WR stars have been analyzed by means of elaborate model atmospheres (cf. Fig. 11), comprising stars in the Milky way, the LMC, the SMC, M33 and a few more nearby galaxies, and thus environments of different metalicities. The obtained stellar and wind parameters provide the empirical basis for understanding the evolution of massive stars, their feedback, and the important role of their population for the ecology of stellar clusters, galaxies, and the whole Universe.

References

Anderson, L. S. 1989, ApJ, 339, 558

Barniske, A., Oskinova, L. M., & Hamann, W.-R. 2008, A&A, 486, 971

Beals, C. S. 1929, MNRAS, 90, 202

Crowther, P. A., Dessart, L., Hillier, D. J., Abbott, J. B., & Fullerton, A. W. 2002, A&A, 392, 653

Gräfener, G. & Hamann, W.-R. 2008, A&A, 482, 945

Gräfener, G., Koesterke, L., & Hamann, W.-R. 2002, A&A, 387, 244

Gräfener, G., Owocki, S. P., & Vink, J. S. 2012, A&A, 538, A40

Hainich, R., Pasemann, D., Todt, H., et al. 2015, A&A, 581, A21

Hainich, R., Rühling, U., Todt, H., et al. 2014, A&A, 565, A27

Hamann, W.-R. 1986, A&A, 160, 347

Hamann, W.-R., Gräfener, G., & Liermann, A. 2006, A&A, 457, 1015

Hamann, W.-R. & Koesterke, L. 1998, A&A, 335, 1003

Hillier, D. J. 1984, ApJ, 280, 744

Hillier, D. J. 2012, in IAU Symposium, Vol. 282, IAU Symposium, ed. M. T. Richards & I. Hubeny, 229

Hummer, D. G. 1962, MNRAS, 125, 21

Liermann, A., Hamann, W.-R., Oskinova, L. M., Todt, H., & Butler, K. 2010, A&A, 524, A82

Martins, F., Hillier, D. J., Paumard, T., et al. 2008, A&A, 478, 219

Mihalas, D., Kunasz, P. B., & Hummer, D. G. 1976, ApJ, 210, 419

Oskinova, L. M., Hamann, W.-R., & Feldmeier, A. 2007, A&A, 476, 1331

Puls, J., Urbaneja, M. A., Venero, R., et al. 2005, A&A, 435, 669

Sander, A., Hamann, W.-R., & Todt, H. 2012, A&A, 540, A144

Sander, A., Todt, H., Hainich, R., & Hamann, W.-R. 2014, A&A, 563, A89

Schmutz, W., Hamann, W.-R., & Wessolowski, U. 1989, A&A, 210, 236

Tramper, F., Gräfener, G., Hartoog, O. E., et al. 2013, A&A, 559, A72

Tramper, F., Straal, S. M., Sanyal, D., et al. 2015, A&A, 581, A110

Šurlan, B., Hamann, W.-R., Aret, A., et al. 2013, A&A, 559, A130

Šurlan, B., Hamann, W.-R., Kubát, J., Oskinova, L. M., & Feldmeier, A. 2012, A&A, 541, A37

Zsargó, J., Hillier, D. J., Bouret, J.-C., et al. 2008, ApJ, 685, L149

Kathryn Neugent: Is there any fundamental difference between CMFGEN and PoWR, and do the results obtained by the two codes generally agree?

Wolf-Rainer Hamann: CMFGEN and PoWR contain the same basic assumptions and physics. However, since the codes have been developed independently, they differ in all possible ways in the numerical details. Since the codes are really complex, it is very valuable to have two codes to compare the results, what we do from time to time. We are not aware of any significant differences so far.

Gloria Koenigsberger: When we look at the temporal sequences of observed lines, such as He II 4686, with a lot of structure attributed to "blobs", is the structure due to emission by the "blobs", absorption, or a combination of both?

Wolf-Rainer Hamann: Both, depending on the line. Those little features drifting on the flat top of, e.g., a C III emission line are pure emission. Drifting features in the P Cygni absorption part of UV resonance lines are pure absorption. And He II 4686 is an emission line which is often optically thick, i.e. here we can have a combination of both, emission and absorption.

Anthony (Tony) Moffat: Is the $\beta = 1$ value determined by fitting or is it adopted? If the latter, then what is the justification, given the observed values of beta from moving clumps in the line-forming regions of many WR stars (Lepine & Moffat 1999) that reveal values $\beta \approx 10$, typically?

Wolf-Rainer Hamann: A velocity law in form of the beta law with exponent $\beta = 1$ is consistent with the observed spectra. However, the model spectra are not very sensitive to the adopted value of β. On one side, this is good news since it means that the derived stellar parameters do not depend much on this assumption. But is also means that we have no handle to determine the velocity law empirically with precision. The hydrodynamical models, as far as available yet, indicate that the beta=1 law is a reasonable approximation for O stars and WNL stars, while for the thick winds from WC stars th elocity law has quite a different shape.